Photorefractive light scattering families in (111)-cut $Bi_{12}TiO_{20}$ crystals with an external electric ac field

V. P. Kamenov,[1] E. Shamonina,[1,2] K. H. Ringhofer,[1] E. Nippolainen,[3] V. V. Prokofiev,[3] and A. A. Kamshilin[3]
[1]*Department of Physics, University of Osnabrück, D-49069 Osnabrück, Germany*
[2]*Department of Engineering Science, University of Oxford, Oxford OX1, 3PJ, United Kingdom*
[3]*Department of Physics, University of Joensuu, P.O. Box 111, FIN-80101 Joensuu, Finland*
(Received 31 July 2000; published 20 December 2000)

We investigate here both theoretically and experimentally light-induced scattering in (111)-cut $Bi_{12}TiO_{20}$ crystals with an external ac field. Our simple analytic solution, which is nearly as precise as the numeric one, allows us to recognize the following otherwise hidden general features. Without the elasto-optic contribution, the scattering patterns are identical for the same value of $\xi=\zeta_0+(2/3)\varphi_p$, where φ_p is the initial polarization angle and ζ_0 is the angle of the external field. With the elasto-optic contribution, the scattering patterns for the same ξ are still very similar. For $\xi\neq 0$, the scattering patterns depend differently on the elasto-optic coefficients p_{12} and p_{13} so that in principle p_{12} and p_{13} can be measured by purely holographic experiments. On the experimental side, we present scattering patterns for $\xi=0$ and $\pm 30°$, showing thereby the similarity of the scattering patterns for equal values of ξ. In all cases, we obtain good qualitative agreement of our analytic and numeric calculations with the experimental findings. [S1063-651X(00)09212-6]

DOI: 10.1103/PhysRevE.63.016607 PACS number(s): 42.70.Nq, 42.65.Hw, 42.70.Ln, 42.40.Pa

I. INTRODUCTION

Light-induced scattering of holographic type in photorefractive crystals is due to formation of secondary noise gratings between light noise, originating from various inhomogeneities, and the pump waves [1]. The scattering may be phase-matched or non-phase-matched. In the first case only those components of the light noise are amplified that are parametrically coupled to the pump waves. In the presence of one pump wave, phase-matched scattering can be realized in crystals with anisotropy [1]. It results in ringlike scattering patterns. The induced birefringence in sillenites is weak even for high applied voltages; therefore non-phase-matched scattering is usually observed [2–4]. That is, many different components of the light noise may be amplified by interaction with the pump wave if the photorefractive response is of nonlocal character. This interaction may be considered as two-wave mixing (TWM) between the pump wave and the individual scattered plane waves if the amplification is weak. In this case the intensity distribution of the scattered light follows the angular dependence of the TWM amplification [5,6], whereby the elasto-optic effect can significantly influence the distribution of the scattered light [2–4,7].

There are a number of publications investigating light scattering in (110)-cut sillenite crystals [2–4,8–10]. But another crystal cut, namely, (111), is attracting more and more interest because it shows the highest possible symmetry [11–15]. The diffusion recording for the (111) cut is studied and optimized in Refs. [13–15]. It is shown there that the thickness dependence of the maximum diffraction efficiency as well as the TWM gain are only on account of the elasto-optic effect. The most interesting cases are when the grating vector is parallel to $[1\bar{1}0]$ or $[11\bar{2}]$ axis [14]. From the symmetry properties, these cases are separated from each other by 30° rotations around the [111] axis. A disadvantage of the (111) cut is its smaller photorefractive response for diffusion recording compared with the (110) cut, but this can be compensated by applying an external electric ac field [16].

In this paper, we investigate photorefractive light scattering governed by TWM processes in (111)-cut $Bi_{12}TiO_{20}$ (BTO) crystals with an external electric ac field, allowing for an arbitrary orientation of the applied electric field. We derive a simple approximate analytical solution that allows us to elucidate general features that are otherwise hidden in many details: There are whole families of related scattering patterns the members of which belong to different directions of the external field and the initial polarization. On the experimental side, we provide scattering patterns for typical representatives of some of those families, showing the similarities within the families. In all cases, we obtain good qualitative agreement of our analytical and numerical calculations with the experimental findings.

II. THEORY

Let a (111)-cut BTO crystal be illuminated by a single linearly polarized pump wave, propagating along the [111] axis. Within the paraxial approximation, the propagation direction of the noise waves is supposed to be close to the [111] axis. An external ac field is applied within the (111) plane. Its temporal profile has a square-wave form with a period much smaller than the grating formation time and much larger than the mobile-electron lifetime. These conditions lead to enhancement of the photorefractive response with an effective energy exchange between the interacting waves [16].

Each weak noise wave can interact with the pump wave and may be amplified by photorefractive TWM. The weakness of the noise waves allows one to use the undepleted pump approximation and guarantees at the same time that the noise waves do not compete with each other. Furthermore, the strong external field makes optical activity ineffective with the exception of those moments when the external field goes through zero so that the optical eigenmodes are practically linearly polarized [3,17]. The following expression for

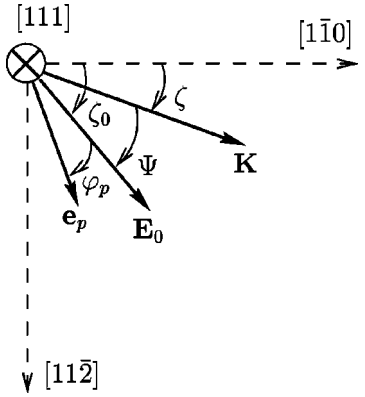

FIG. 1. Optical configuration of (111)-cut crystals.

the amplitude $\mathbf{A}_s$ of the weak wave is derived in Ref. [3]: $\mathbf{A}_s(d)\cdot\mathbf{e}_p=\mathbf{A}_s(0)\cdot\mathbf{e}_p\exp(\gamma d)$, where $\mathbf{e}_p$ is the polarization vector of the pump wave and d is the crystal thickness. The increment γ characterizes the energy exchange and depends on the particular experimental conditions (crystal cut, thickness, and initial light polarization) as well as on the propagation direction of the weak wave. The intensity of the noise wave will grow exponentially with the thickness if $\gamma>0$. Therefore the structure of the scattering pattern on the rear side of the crystal follows the spatial distribution of the exponential increment $\gamma>0$. Following Ref. [3], we arrive at

$$\gamma=\Gamma+C_1\frac{\sin 2\kappa d}{d} \tag{1}$$

with $\kappa=s|E_0|\sqrt{6}/3$. Here E_0 is the amplitude of the external electric field and the coefficient $s=-\pi n_0^3 r_{41}^S/\lambda$ depends on the refractive index n_0, the clamped electro-optic coefficient r_{41}^S, and the wavelength λ. For the (111) cut we obtain

$$\Gamma=s|E_0\cos\psi|Q[h_1+(h_2\sin 3\beta+h_3\cos 3\beta)\sin 3\xi], \tag{2}$$

$$C_1=-(\sqrt{6}/4)Q|\cos\psi|(h_2\cos 3\beta-h_3\sin 3\beta)\cos 3\xi, \tag{3}$$

where $\beta=\zeta_0-(2/3)\psi$ and $\xi=\zeta_0+(2/3)\varphi_p$. The angles ζ_0 and ψ define the orientation of the external field and the grating vector (see Fig. 1); φ_p is the polarization angle of the pump wave. The coefficients $h_1=H_{xx}+H_{yy}$, $h_2=H_{xx}-H_{yy}$, and $h_3=2H_{xy}$ depend on the dimensionless components of the coupling tensor H_{ij}, which are proportional to the induced change of the inverse dielectric permittivity tensor [15]. The quality factor Q depends on ψ and is given by

$$Q=\left(\frac{|E_0\cos\psi|}{E_q}+\frac{E_D+E_M}{|E_0\cos\psi|}\right)^{-1}, \tag{4}$$

where E_D, E_q, and E_M are the characteristic fields [3].

In the coordinate system with x axis parallel to the grating vector the components H_{ij} can be presented in a simple form with an accuracy of 4% [15]:

$$H_{xx}=a_{xx}\sin 3\zeta,\quad H_{yy}=a_{yy}\sin 3\zeta,\quad H_{xy}=a_{xy}\cos 3\zeta, \tag{5}$$

TABLE I. Optical and material parameters of BTO for $\lambda=632.8$ nm [18]. n_0 is the refractive index; ε is the dielectric permittivity; p_{ij}^E, c_{ij}^E, e_{14}, and r_{41}^S are the nonzero components of the elasto-optic, elastic, piezoelectric, and electro-optic tensors, respectively.

n_0	ε	r_{41}^S (pm/V)	c_{11},c_{12},c_{44}^E (10^{10}N/m^2)	$p_{11},p_{12}+p_{13},p_{44}^E$	e_{14} (C/m^2)
2.58	47	4.75	12.5, 2.75, 2.42	-0.055, 0.295, 0.0035	1.1

where $\zeta=\zeta_0-\psi$ is the angle between the [1$\bar{1}$0] axis and the grating vector (see Fig. 1). If only the electro-optic effect is taken into account, we have $a_{xx}=a_{xy}=-a_{yy}=\sqrt{6}/3$. With the elasto-optic contribution, the result is $a_{xx}\simeq 1.16$, $a_{xy}\simeq 0.83$, and $a_{yy}\simeq -0.76$. The values of a_{ij} are calculated using the material constants from Table I.

The coefficient Γ from Eq. (1) is responsible for a monotone amplification of the weak wave while the term proportional to C_1 leads to intensity oscillations with the crystal thickness d. The thickness dependence of the increment γ is due to the change of light polarization within the crystal. In our case, this change is mainly caused by the induced birefringence. The variation of the light polarization results in a variation of the effective coupling between the interacting waves. Therefore, the total energy exchange becomes thickness dependent. This is analogous to the case of diffusion recording where the thickness dependence of the gain is due to the rotation of the light polarization owing to optical activity [3,18]. Note, however, that in the ac case with large amplitude of the applied field, the optical eigenmodes are essentially linearly polarized. Thus by choosing a proper input linear polarization, we can excite only one eigenmode so that the light polarization remains constant within the crystal. In this special case, we have $C_1=0$, i.e., the increment γ is thickness independent.

Being proportional to E_0, Γ can lead to a very strong amplification if the amplitude of the applied electric field is large. C_1 does not depend on E_0 at all and cannot lead to strong noise amplification. Since both coefficients are ζ_0 and φ_p dependent, there are optical configurations with Γ much larger than C_1 and others with Γ negligible compared with C_1 even for large E_0.

Equations (5) further simplify to

$$\Gamma=s|E_0\cos\psi|Q(b_1\sin 3\zeta+b_2\cos\psi\sin 3\xi), \tag{6}$$

$$C_1=(\sqrt{6}/4)Q|\cos\psi|b_2\sin\psi\cos 3\xi, \tag{7}$$

where $b_1=a_{xx}+a_{yy}\simeq 0.4$ and $b_2=a_{xy}+(a_{xx}-a_{yy})/2\simeq 1.8$.

It can be proved directly that the symmetries $\Gamma(\zeta_0\pm 120°)=\Gamma(\zeta_0)$ and $C_1(\zeta_0\pm 120°)=C_1(\zeta_0)$ hold true because of the threefold symmetry, typical for (111)-cut crystals of the sillenite family. It is important to note that there is no such symmetry with respect to ψ since this angle is not measured from any crystallographic axis. For this reason the azimuthal distribution of the increment γ (or of the scattering pattern) will generally not have a threefold symmetry.

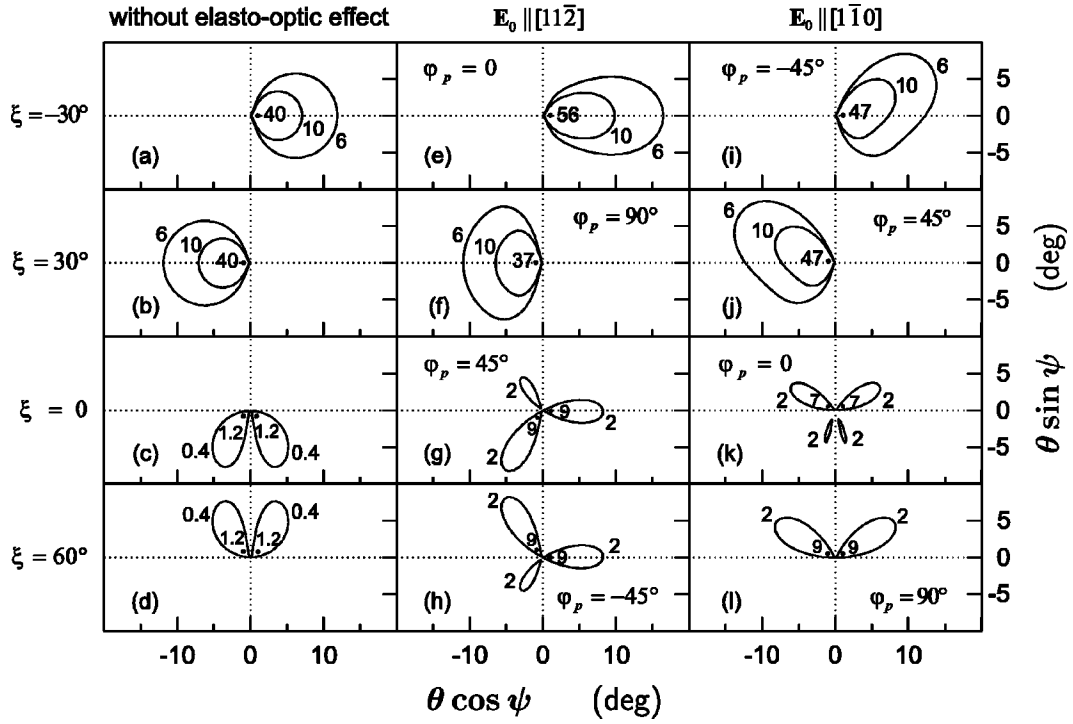

FIG. 2. Contour plots of the increment $\gamma(\theta,\psi)>0$. The left column corresponds to the case without elasto-optic effect, the central and the right to $\mathbf{E}_0 \| [11\bar{2}]$ and $\mathbf{E}_0 \| [1\bar{1}0]$, respectively. On the left-hand side of each row is indicated the value of the corresponding angle ξ. The contours are calculated from Eqs. (2),(3) with material parameters from Table I and a crystal thickness $d=5.1$ mm.

Formulas (6) and (7) give results only slightly different from the numerical solution; their great advantage is that they allow recognition of important general features that are otherwise hidden in a jungle of formalism. In what follows, we consider first conventional TWM with the grating vector parallel to the external field, then we analyze the scattering properties neglecting the elasto-optic contribution, and, finally, we take the elasto-optic contribution into account.

With the help of Eq. (6), we can find the optimum orientation for the conventional TWM experiment where the grating vector is parallel to the applied electric field. For this purpose we set $\psi=0$ and see from Eq. (7) that $C_1=0$. After optimization with respect to the polarization angle of the pump wave φ_p, we obtain

$$\Gamma|_{\varphi_p}^{\max} = s|E_0|Q(b_1 \sin 3\zeta_0 + b_2). \tag{8}$$

The corresponding optimum initial light polarization $\varphi_p^{\max}$ depends linearly on the orientation ζ_0 of the external field, $\varphi_p^{\max}=45°-(3/2)\zeta_0$. The absolute maximum $\Gamma^{\max}=s|E_0|Q(b_1+b_2)$ is achieved for $\zeta_0^{\max}=90°$ and $\varphi_p^{\max}=0$, i.e., the external field and the electric field of the pump wave are along the $[11\bar{2}]$ axis.

Depending on the direction of the external field and on the initial light polarization, the main lobe of the scattered light will be, in general, not parallel to the applied electric field. It turns out, however, that the conditions for the strongest scattering coincide with those for the strongest energy exchange for the conventional TWM: $\zeta_0^{\max}=90°$ and $\varphi_p^{\max}=0$.

For the convenience of the reader we refer in advance to Fig. 2 which summarizes the scattering patterns discussed below. Each of Figs. 2(a)–2(l) shows the angular distribution of the increment $\gamma(\theta,\psi)>0$, with the angle θ measured between the propagation directions of the pump wave and the signal wave.

Without the elasto-optic effect, Eqs. (2) and (3) take the form

$$\Gamma^0 = 2(\sqrt{6}/3)s|E_0 \cos\psi|Q \cos\psi \sin 3\xi, \tag{9}$$

$$C_1^0 = (\sqrt{6}/4)Q|\cos\psi|\sin\psi \cos 3\xi. \tag{10}$$

From Eqs. (9) and (10) it follows that without the elasto-optic contribution the scattering patterns are identical for the same value of $\xi=\zeta_0+(2/3)\varphi_p$. Thus any given ξ determines a family of identical scattering patterns, the members of which belong to different directions of the external field and of the initial polarization. Of special interest are the following two types of families.

(1) The Γ families with $\xi=\mp 30°$ [see Figs. 2(a) and 2(b)], corresponding to $\mathbf{E}_0 \| [11\bar{2}]$ with $\varphi_p=0°$ and 90°, respectively, and to $\mathbf{E}_0 \| [1\bar{1}0]$ with $\varphi_p=\mp 45°$. These families are characterized by $C_1=0$. They provide the most intensive scattering (''one lobe'' pattern). The figures are related by reflection with respect to the horizontal axis since $\Gamma^0(\xi=30°)=-\Gamma^0(\xi=-30°)$ and $\Gamma^0(\psi+180°)=-\Gamma^0(\psi)$.

(2) The C_1 families with $\xi=0$ and 60° [see Figs. 2(c) and 2(d)], corresponding to $\mathbf{E}_0 \| [11\bar{2}]$ with $\varphi_p=\pm 45°$ and to $\mathbf{E}_0 \| [1\bar{1}0]$ with $\varphi_p=0°$ and 90°, respectively. For these

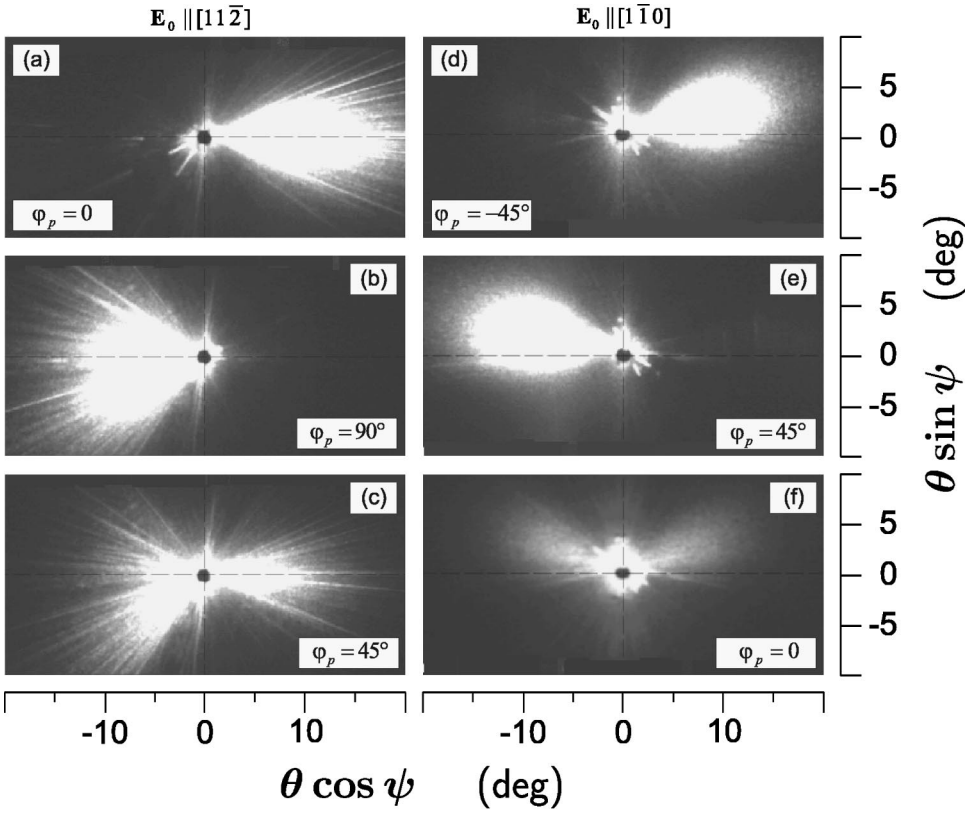

FIG. 3. Experimental observation of light-induced scattering for the cases $\mathbf{E}_0 \| [11\bar{2}]$ (first column) and $\mathbf{E}_0 \| [1\bar{1}0]$ (second column). In the case $\mathbf{E}_0 \| [11\bar{2}]$, the scattering pattern for $\varphi_p = -45°$ is essentially the same as the pattern for $\varphi_p = 45°$ [the latter is shown in (c)]. In the case $\mathbf{E}_0 \| [1\bar{1}0]$, the scattering pattern for $\varphi_p = 90°$ is practically the same as the pattern for $\varphi_p = 0$ [the latter is shown in (f)].

families, $\Gamma = 0$, and the scattering pattern is extremely weak (''tiny butterfly'' pattern). The figures are related by reflection with respect to the vertical axis since $C_1^0(\xi = 0) = -C_1^0(\xi = 60°)$ and $C_1^0(\psi + 180°) = -C_1^0(\psi)$.

We emphasize that the scattering patterns are determined by the parameter ξ and can therefore be observed for any crystal orientation.

The elasto-optic contribution does not change this general picture of the scattering families. The elasto-optic contribution, however, modifies each figure of one and the same family in a different way, so that the scattering patterns within one family are not identical but similar.

It turns out that, unlike Γ, C_1 is not strongly affected by the elasto-optic contributions. In particular, for the C_1 families, Γ exceeds C_1 so that mostly Γ determines the scattering although C_1 is not negligibly small. A direct calculation shows that for these families Γ depends essentially only on the sum $p_{11} + p_{12} + p_{13} + p_{44}^E$ of elasto-optic coefficients. On the other hand, for the Γ families, $C_1 = 0$. For these families, Γ depends not only on the sum $p_{12} + p_{13}$ but also on $p_{12} - p_{13}$. This offers the possibility of determining p_{12} and p_{13} by purely holographic measurements. This would be impossible with the (110) cut for which only the sum of p_{12} and p_{13} appears.

Let us now consider light scattering for the two practically important cases with the field applied either along the $[11\bar{2}]$ axis ($\zeta_0 = 90°$) or along the $[1\bar{1}0]$ axis ($\zeta_0 = 0°$). The coefficient C_1 is zero for the Γ families [see both upper figures of the central and right columns in Fig. 2 (''one lobe'' pattern)]. C_1 is not negligible for the C_1 families [see both lower figures of the central and right columns in Fig. 2 (''cloverleaf'' and ''butterfly'' patterns, respectively)]. Since $\Gamma(\xi = 0°) = \Gamma(\xi = 60°)$, the difference between the scattering in Figs. 2(g) and 2(h) and between Figs. 2(k) and 2(l) is due to the coefficient C_1. If we neglect C_1 (i.e., if the crystal is thick), the individuals in each pair become identical: the upper and the lower lobes of the ''cloverleaves'' [Figs. 2(g) and 2(h)] become symmetric; the ''butterflies'' in Figs. 2(k) and 2(l) remain both with upper wings only. Since $C_1 = 0$ for $\xi = \mp 30°$, the difference in shape between Figs. 2(e) and 2(f) and between Figs. 2(i) and 2(j) are only on account of the elasto-optic effect.

III. COMPARISON WITH EXPERIMENT

We measured the light-scattering patterns in a BTO crystal with dimensions $2.11 \times 4.97 \times 5.07$ mm^3 with applied field along $[11\bar{2}]$ and in a BTO crystal with dimensions $2.63 \times 6.4 \times 5.16$ mm^3 with applied field along the $[1\bar{1}0]$ axis. The first numbers are the distances between the electrodes and the last ones are the crystal thicknesses. Silver electrodes were deposited along the whole crystal thickness. A laser beam of wavelength $\lambda = 632.8$ nm, diameter 1.4 mm, and intensity about 1.2 W/cm^2 was normally incident onto the sample. The amplitude of the square-wave electric ac field was 20 kV/cm. The scattering patterns were recorded in the far field with a charge-coupled device camera.

Figures 3(a)–3(f) show the light-scattering patterns obtained for different inclinations of the pump wave polarization. The maximum scattering is obtained for $\mathbf{E}_0 \| [11\bar{2}]$ and $\varphi_p = 0$, which corresponds to our analysis. In agreement with theory, we have the one lobe structure for $\xi = \mp 30°$ [com-

pare the pairs Figs. 3(a),3(b) with Figs. 2(e),2(f) and Figs. 3(d),3(e) with Figs. 2(i), 2(j), respectively]. The patterns ''cloverleaf'' and ''butterfly'' can be recognized in Figs. 3(c) and 3(f) [compare with the pairs Figs. 2(g),2(h) and Figs. 2(k),2(l), respectively].

Looking in more detail at Figs. 2 and 3, we see that there is a small asymmetry in the experimental results for $\mathbf{E}_0 \| [11\bar{2}]$ and $\varphi_p = 90°$. The intensity of the lower part of the scattering pattern in Fig. 3(b) is stronger, which is not predicted from the theoretical results. Similarly, the lower lobe of the experimental results for $\mathbf{E}_0 \| [11\bar{2}]$ and $\varphi_p = \pm 45°$ is stronger than the upper one [see Fig. 3(c) and the figure caption. At the same time, according to theory, the upper lobe should be stronger for $\varphi_p = -45°$.

We point out a few possible sources for the discrepancy between theory and experiment. First, there may be an error in the crystal cut (i.e., uncertainty in the plane of incidence and external field orientation). The theoretical simulations show that varying the propagation direction from the [111] axis by less than 5° results in the asymmetrical pattern of Fig. 3(b) and 3(c). We could not, however, prove this assumption experimentally. Tilting the crystal with the aim of compensating possible errors of the crystal cut (estimated to be less than 5°) did not lead to any remarkable change of the structure of Figs. 3(b) and 3(c). Moreover, we performed the same experiment with several (111)-cut BTO crystals and always obtained similar scattering pictures, which remained insensitive to rotation.

Another possible source for the observed discrepancy between theory and experiment can be hidden in the existing set of material constants. TWM experiments in (110)-cut BTO crystals have been performed to determine the elasto-optic coefficients [19,18]. Since the photorefractive effect for this cut depends on the sum of the elasto-optic coefficients p_{12} and p_{13}, the separate values of this coefficients are not known. A characteristic feature of the (111) cut is that p_{12} and p_{13} are no longer equivalent and that both must be known. In our calculations we used the coefficients from Ref. [18] (see Table I) and supposed that $p_{12} = p_{13}$, although for the crystals of the (23) point group this assumption may be wrong. Note that the coefficient Γ from Eq. (2) depends also on the difference $p_{12} - p_{13}$ if $\xi = \pm 30°$ and does not depend on it if $\xi = 0$ or 60°. Consequently, while the possibly different values of p_{12} and p_{13} can explain the asymmetry of Fig. 3(b) they cannot explain the equivalence of the cases $\varphi_p = \pm 45°$ from Fig. 3(c).

Finally, the simplified model might be insufficient to provide complete agreement with the experiment. Although scattering is a very complex multiple-wave-mixing process, we describe it by a simple TWM model in the framework of the undepleted pump approximation. Full agreement with the experimental data can never be expected.

An important result of our study is that we classified theoretically and verified experimentally families of the scattering pictures, grasped their main features, and proposed the possibility of determining p_{12} and p_{13} independently of each other. The simple analytical expressions derived above may be useful in planning a TWM experiment with the aim of an accurate measurement of p_{12} and p_{13} by a pure holographic method.

IV. CONCLUSIONS

In conclusion, we have investigated analytically and experimentally the process of photorefractive wave mixing governed by TWM processes in (111)-cut BTO crystals. Theoretically we found the optimum orientation for TWM and analyzed the light-induced scattering for different orientations of the external field and light polarization. The contribution of the elasto-optic effect was also discussed. It was pointed out that the (111) cut can be used for measurements of the elasto-optic coefficients p_{12} and p_{13}, which up to now are unknown for BTO crystals. The theoretical results are in good qualitative agreement with experiment.

ACKNOWLEDGMENTS

We thank O. V. Kobozev for assistance in the experiment and acknowledge the financial support of the Deutsche Forschungsgemeinschaft [Sonderforschungsbereich 225 and Emmy-Noether Program (Germany)] and the Volkswagen Stiftung (Project No. Az I/72 919).

[1] L. Solymar, D. J. Webb, and A. Grunnet-Jepsen, *The Physics and Applications of Photorefractive Materials* (Clarendon, Oxford, 1996), pp. 269–281.
[2] H. C. Ellin and L. Solymar, Opt. Commun. **130**, 85 (1996).
[3] B. I. Sturman, E. V. Podivilov, K. H. Ringhofer, E. Shamonina, V. P. Kamenov, E. Nippolainen, V. V. Prokofiev, and A. A. Kamshilin, Phys. Rev. E **60**, 3332 (1999).
[4] H. Tuovinen, A. A. Kamshilin, and J. Jaaskelainen, J. Opt. Soc. Am. B **14**, 3383 (1997).
[5] V. V. Voronov, I. R. Dorsh, Y. S. Kuz'minov, and N. V. Tkachenko, Kvant. Electron. (Moscow) **7**, 2313 (1980) [Sov. J. Quantum Electron. **10**, 1346 (1980)].
[6] N. D. Khat'kov and S. M. Shandarov, Autometrija **2**, 61 (1983) (in Russian).
[7] G. Montemezzani, A. A. Zozulya, L. Gzaia, D. Z. Anderson, M. Zgonik, and P. Günter, Phys. Rev. A **52**, 1791 (1995).
[8] H. C. Ellin, J. Takacs, and L. Solymar, Appl. Opt. **33**, 4125 (1994).
[9] H. Rajbenbach and J. P. Huignard, Opt. Lett. **10**, 137 (1985).
[10] H. Rajbenbach, A. Delboulbé, and J. P. Huignard, Opt. Lett. **14**, 1275 (1989).
[11] B. Sugg, F. Kahmann, R. A. Rupp, P. Delaye, and G. Roosen, Opt. Commun. **102**, 6 (1993).
[12] N. Kukhtarev, B. S. Chen, P. Venkateswarlu, G. Salamo, and M. Klein, Opt. Commun. **104**, 23 (1993).
[13] V. V. Shepelevich, S. F. Nichiporko, A. E. Zagorskiy, N. N. Egorov, Y. Hu, K. H. Ringhofer, and E. Shamonina, OSA Trends Opt. Photonics Ser. **27**, 353 (1999).

[14] E. Shamonina, Y. Hu, V. P. Kamenov, K. H. Ringhofer, V. Y. Gayvoronsky, S. F. Nichiporko, A. E. Zagorskiy, N. N. Egorov, and V. V. Shepelevich, Opt. Commun. **180**, 183 (2000).

[15] V. P. Kamenov, Y. Hu, E. Shamonina, K. H. Ringhofer, and V. Y. Gayvoronsky, Phys. Rev. E **62**, 2863 (2000).

[16] S. I. Stepanov and M. P. Petrov, Opt. Commun. **53**, 292 (1985).

[17] E. Shamonina, K. H. Ringhofer, B. I. Sturman, V. P. Kamenov, G. Cedilnik, M. Esselbach, A. Kiessling, R. Kowarschik, A. Kamshilin, V. Prokofiev, and T. Jaaskelainen, Opt. Lett. **23**, 1435 (1998).

[18] S. M. Shandarov, A. Emelyanov, O. Kobozev, A. Reshet'ko, V. V. Volkov, and Y. F. Kargin, Proc. SPIE **2801**, 221 (1996).

[19] S. I. Stepanov, S. M. Shandarov, and N. D. Khat'kov, Fiz. Tverd Tela (Leningrad) **29**, 3054 (1987) [Sov. Phys. Solid State **29**, 1754 (1987)].